High Blood Pressure & Cardiovascular Prevention (2024) 31:299–308
https://doi.org/10.1007/s40292-024-00641-5

ORIGINAL ARTICLE

Intracellular Calcium Dynamics in Primary Human Adrenocortical Cells Deciphered with a Novel Pipeline

Hala Ajjour[1] · Giorgia Pallafacchina[2] · Livia Lenzini[1] · Brasilina Caroccia[1] · Gian Paolo Rossi[1]

Received: 27 February 2024 / Accepted: 2 April 2024 / Published online: 20 May 2024

Abstract

Introduction The fluctuations of the intracellular Ca^{2+} concentration ($[Ca^{2+}]_i$) are key physiological signals for cell function under normal conditions and can undergo profound alterations in disease states, as high blood pressure due to endocrine disorders like primary aldosteronism (PA). However, when assessing such fluctuations several parameters in the Ca^{2+} signal dynamics need to be considered, which renders their assessment challenging.

Aim Aim to develop an observer-independent custom-made pipeline to analyze Ca^{2+} dynamics in terms of frequency and peak parameters, as amplitude, full width at half maximum (FWHM) and area under the curve (AUC).

Methods We applied a custom-made methodology to aldosterone-producing adenoma (APA) and APA adjacent cells (AAC) and found this pipeline to be suitable for monitoring and processing a wide-range of $[Ca^{2+}]_i$ events in these cell types delivering reproducible results.

Conclusion The designed pipeline can provide a useful tool for $[Ca^{2+}]_i$ signal analysis that allows comparisons of Ca^{2+} dynamics not only in PA, but in other cell phenotypes that are relevant for the regulation of blood pressure.

Keywords Intracellular calcium dynamics · Adrenocortical cells · Aldosterone producing Adenoma · Calcium peak detection · Calcium signal decoding

1 Introduction

As a key second messenger, Ca^{2+} regulates a wide range of cellular processes, including gene expression, endocrine secretion, muscle contraction and synaptic transmission [1, 2]. In fact, fluctuations in intracellular Ca^{2+} concentration ($[Ca^{2+}]_i$) are pleiotropic signals for the orchestration of pathways regulating cell functions under both physiological and pathophysiological conditions [3–5].

The dynamics of $[Ca^{2+}]_i$ changes is complex and variable, depending on the origin of the stimulus and triggering signal, the cell type and the specific cell state [6, 7]. Moreover, stimuli of different origins generate specific Ca^{2+} signals with peculiar amplitude and frequency, decoded by different downstream Ca^{2+}-sensitive proteins and different signaling pathways [3, 8].

Primary aldosteronism (PA), the most common cause of endocrine hypertension, is commonly caused by aldosterone-producing adenoma (APA), which induces an autonomous aldosterone production due to a set of somatic or germline mutations in ion channel and pump genes that ultimately lead to an increase in $[Ca^{2+}]_i$ of aldosterone-producing cells [9–11]. When due to APA, PA is surgically curable by adrenalectomy. Adrenocortical cells rely on Ca^{2+} for the regulation of early and late limiting steps of steroidogenesis since Ca^{2+} elevation induces the transport of cholesterol to the Cytochrome P450 Family 11 Subfamily A Member 1 (CYP11A1) in the inner mitochondrial membrane (IMM), and stimulates aldosterone synthase (CYP11B2) gene expression via activation of calmodulin and Ca^{2+}/calmodulin-dependent protein kinases [12–14].

Studies had investigated Ca^{2+} signaling dynamics in aldosterone-producing cells in rodents *ex vivo* and in adrenocortical cell lines [7, 15–22]. Some have reported a high

✉ Gian Paolo Rossi
gianpaolo.rossi@unipd.it

[1] Specialized Center of Excellence for Hypertension of the European Society of Hypertension and Emergency Medicine Unit, Department of Medicine-DIMED, University Hospital, University of Padua, Padua 35126, Italy

[2] Neuroscience Institute, Italian National Research Council (CNR) and Department of Biomedical Sciences, University of Padua, Padua 35131, Italy

cell-cell variability of Ca^{2+} signals, while others have provided quantitative Ca^{2+} trace processing by implementing computational models [19–22]. However, the algorithms utilized for the analyses of the recorded Ca^{2+} levels were not consistent and reproducible, which highlighted the need for a standardized methodology for the assessment of adrenal cell $[Ca^{2+}]_i$ dynamics in response to physiological stimuli as well as in pathological conditions.

We, therefore, sought for developing an observer-independent methodology for the analysis of $[Ca^{2+}]_i$ dynamics in isolated human CD56+ adrenocortical cells by quantitatively monitoring intracellular Ca^{2+} levels using the Ca^{2+}-sensitive-indicator Fura-2 in resting conditions and after challenging them with Angiotensin II, one of the most potent physiological aldosterone secretagogues [23]. To provide standardized protocol for the analysis, we optimized a computational methodology that quantitatively assess Ca^{2+} signal recordings of individual adrenocortical cells over time, from a large data set without the need for advanced coding skills or sophisticated computer programs.

2 Methods

2.1 Cell Preparation and Culture

APA and APA adjacent tissues were collected in the operating room, cleared from surrounding fat and connective tissue, cells were mechanically and chemically dispersed and immune magnetically separated with anti-CD56 (neural cell adhesion molecule) antibody pre-coated magnetic beads as reported [24].

CD56+ cells, isolated according to methods of Caroccia et al. [24], were checked for viability using trypan blue and seeded on 24 mm poly-lysinated glass coverslips 24 h prior to Ca^{2+} imaging experiment in DMEM/F-12 (Dulbecco's Modified Eagle Medium/Nutrient Mixture F-12) supplemented with 1% Penicillin/Streptomycin, 1 % Insulin-Transferrin-Selenium (ITS), and 5 % cosmic calf serum (CCS).

The collection of samples was approved by the local ethics committee. Recruited patients provided signed consents.

2.2 Ca^{2+} Imaging

The day of experiment, CD56+ cells were washed twice with modified Krebs-Ringer Buffer (KRB) consisting of NaCl (135 mM), KCl (2.5 mM), $MgSO_4$ x 7H2O (1 mM), $MgCl_2$ x 6H2O (1 mM), K_2HPO_4 (0.4 mM), HEPES (20 mM), glucose (5.5 mM), and $CaCL_2$ (1 mM) at pH 7.4. Afterwards, cells were incubated with 2 µM Fura-2-AM (Life Technologies, Milan, Italy) for 20 minutes at 37 °C in KRB added with 0.02% Pluronic acid and 250 µM sulphinpyrazone. After one wash with KRB, cells were transferred to a metal open-top holder and placed on the microscope stage for image acquisition. After acquisition of basal resting Fura-2 signal, cells were treated with Ang II at different doses (0.1 nM, 1 nM, 10 nM), then ATP (100 µM), and ionomycin (1 µM) were added to induce IP3-dependent ER Ca^{2+} release and to permeabilize plasma membrane in order to saturate the Ca^{2+} dye, respectively. Ca^{2+}-dependent Fura-2 fluorescence levels was monitored using an inverted fluorescence microscope Nikon Eclipse Ti equipped with a Zyla-CMOS 4.2-P camera (Andor, Oxford Instruments, Abingdon, UK) and a 40x objective Nikon S Fluor Oil 1.30 DIC H/N2 WD 0.22). Excitation wavelengths were obtained with a 75 W Xenon Lamp (USHIO, UXLS50A) and a monochromator (Cairn Optoscan Monochromator, Cairn Research Ltd., Faversham, UK) controlled by NIS-ELEMENTS AR (Nikon) software provided alternating excitation wavelengths (340/380 nm). A neutral density filter, ND4 (Nikon, USA) and a FF-409-DiO3 Dichroic (Semrock) were used in the excitation pathway. Collection of emitted fluorescence was done using a 510/84 nm filter (Semrock). Images were acquired every 1 s with 100 ms exposure time, by a Zyla-CMOS 4.2-P (Andor, Oxford Instruments) controlled by the same software.

2.3 Data Processing and Workflow

A custom-made pipeline was developed to analyze the variations in individual cell Ca^{2+} signals assessed by Fura-2 (Fig. 1). The input was a confocal microscope image and the resulting output was distinct individual peaks with peak parameters associated to each. The pipeline enclosed 3 main steps: 1) data extraction and construction, 2) trace plotting and peak identification and 3) peak filtering.

We used ImageJ-based Fiji software, Microsoft Excel 2019 MSO (Version 2304 Build 16.0.16327.20200), and OriginPro 2023 software (10.0.0.154 academic version, OriginLab Corporation, Northampton, MA, USA-).

Data extraction was executed manually on ImageJ-based Fiji image analysis software by assigning individual cell as a region of interest (ROI) on raw confocal images (Fig. 2). Fura-2 is a dual excitation ratiometric Ca^{2+} indicator commonly used for the measurements of intracellular $[Ca^{2+}]$. The Ca^{2+}-free form of Fura-2 has a peak excitation wavelength at ~ 380 nm, whereas the Ca^{2+}-bound form has a peak excitation wavelength at ~ 340 nm. An elevation of Ca^{2+} concentration induces an increase in Fura-2 emission fluorescence when the indicator is excited at 340 nm, with a corresponding decrease in fluorescence at 380-nm excitation. The ratio between emission after excitation at 340 nm and 380 nm (340/380 ratio) represents a good estimation of the level of Ca^{2+} in the sample [25]. The fluctuations of Fura-2 fluorescence emission at the 2 different exciting wavelengths (340 nm and 380 nm) were recorded and

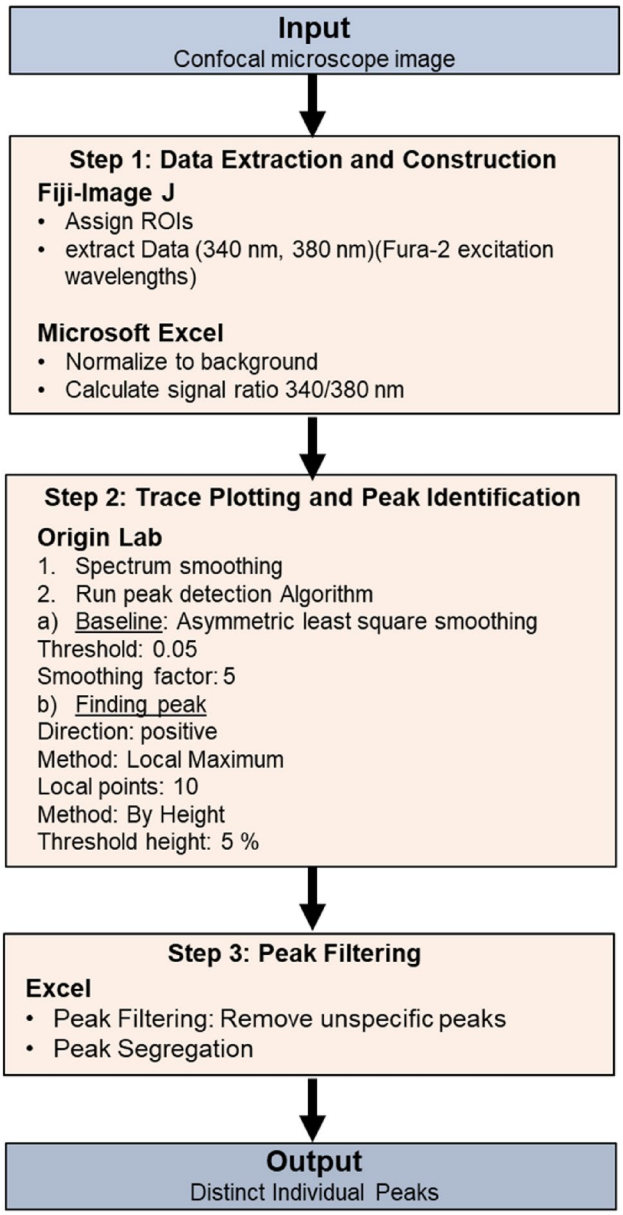

Fig. 1 Workflow of custom-made peak detection pipeline. Input data are the raw confocal microscope images of the Ca^{2+}-sensitive probe fluorescence and the output results are dynamics parameters (number, frequency and shape) of individual cell Ca^{2+} peaks. The pipeline comprises 3 data processing steps. Step 1 (Data Extraction and Construction): assignment of ROIs, extraction of Fura-2 signal value for the two excitation wavelengths (Fiji-Image J), normalization of data to the background, and calculation of Fura-2 340/380 nm signal ratios (Microsoft Excel). Step 2 (Trace Plotting and Peak Finding): data smoothing followed by peak detection through the application of the OriginPro software algorithm. Step 3 (Peak Filtering): implementation of Microsoft Excel's equations to identify spontaneous vs Ang II-evoked Ca^{2+} peaks. For Ang II-evoked peaks, first and subsequent oscillations are considered separately

extracted separately, each normalized to the relative background noise (a region of the coverslip devoid of cells), then expressed as 340/380 ratio.

3 Results

3.1 Trace Plotting and Peak Identification

Ca^{2+} traces were plotted using OriginPro lab software. However, some samples present undesired background fluctuations that were reduced by applying a noise reduction algorithm based on the Savitzky-Golay (SG) method to all sample traces [26–28]. The SG method fits a polynomial regression to successive data points of a moving window (local least-squares polynomial approximation) to recover the trace shape. The degree of smoothness was optimized at a window size = 20 which resembles the number of data points used in each local regression. The mentioned data processing tool achieves data smoothing while preserving the distinct features and properties of various data patterns and frequencies. The mentioned settings have been determined for few traces selected as templates and then used in the following batch analysis for the required large data set.

As shown in Fig. 3, in both AAC and APA cells, the Ca^{2+} signals do not always return to the baseline level after Ang II stimulation. Thus, establishing of a straight-line baseline functional to the event detection is rather inefficient. Therefore, a critical step towards processing dynamic live cell recordings is to adopt a baseline calculation approach capable to drift and adapt to the peculiarity and specificity of the signal of each cell. Accordingly, to estimate the baseline, we implemented the "Asymmetric least square smoothing baseline setting" (ALS) in the peak detection algorithm of OriginPro software. A threshold at 0.05, smoothing factor at 5, with a number of iterations set at 10 were the parameters implemented to run the algorithm. These settings correct the baseline by asymmetrically weighting the trace deviations and the estimated baseline adjusts to the highly dynamic $[Ca^{2+}]_i$ oscillations, allowing to adapt to the drift in signals (Fig. 4a). The settings of the peak finding algorithm were set as follows: Direction = positive; Method = Local Maximum; Local points=10. In addition to that, the algorithm promoted detection of peaks following the indicated peak filtering settings: Method = By Height; Threshold height= 5 %.

We focused our analysis on selected peak features, defined as: (i) amplitude from baseline (height of the peak), (ii) area under the curve (AUC, which represents an estimation of the total amount of Ca^{2+} entering the cell) and (iii) full width at half maximum (FWHM, which describes the extension/duration of the peak (Fig 4b). The results of the optimized algorithm described are identified individual peaks (Fig 5a–d).

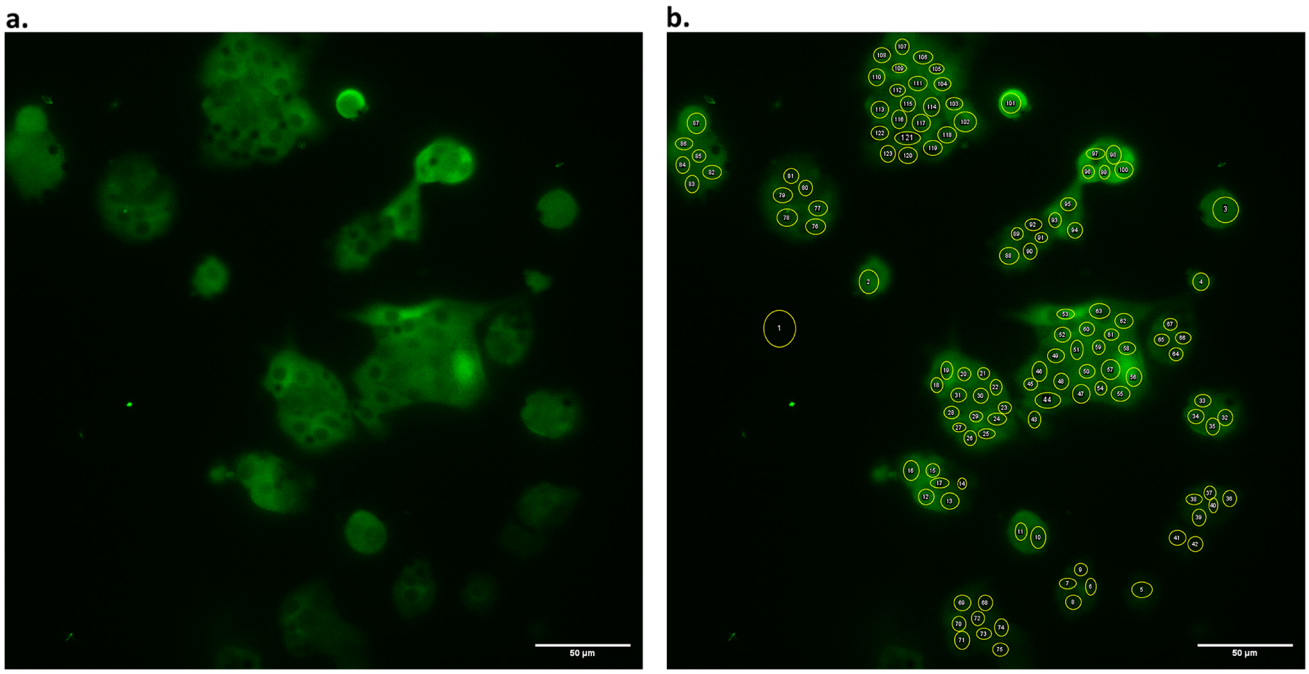

Fig. 2 Representative confocal image of CD56+ cell after 24 hours in culture. **a** Raw image, **b** same as A after ROIs assignment. Black dots represent anti-CD56+ magnetic beads used for cell isolation. ImageJ-based Fiji software was utilized to assigned ROIs. Scale bar = 50 µM

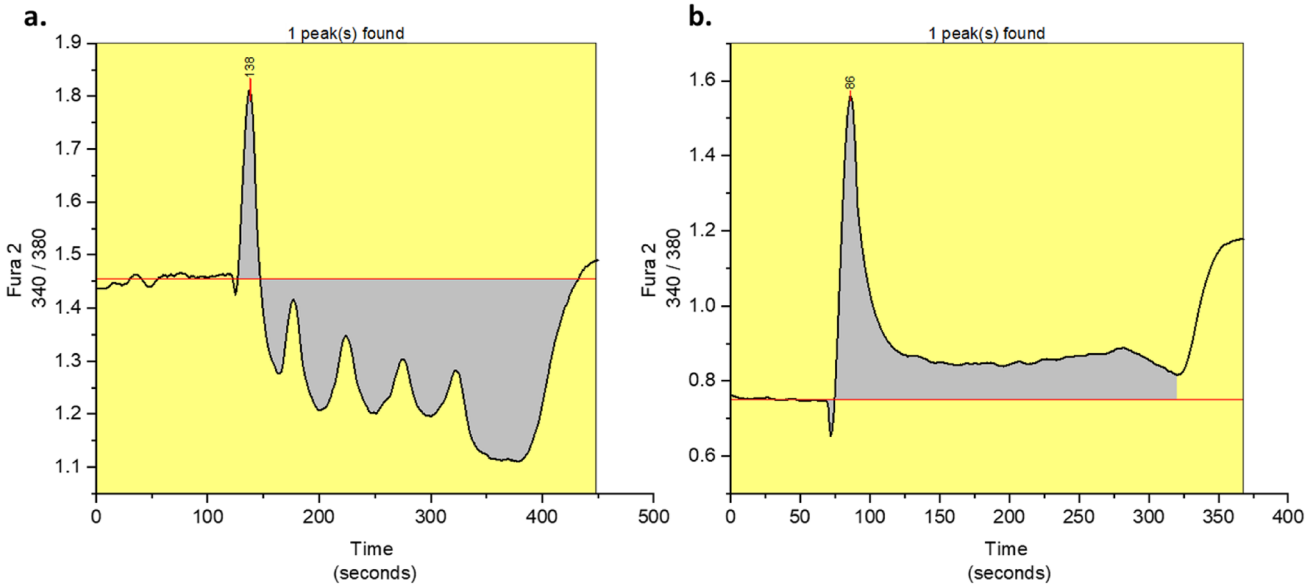

Fig. 3 Baseline detection. **a**, **b** Representative Ca^{2+} signal traces of 2 different AAC showing the inadequacy of setting a straight-line (red line) as baseline when performing dynamic Ca^{2+} recordings and peak detection. In these samples, the set baseline vanishes the detection of oscillations (left panel) and fails to accurately detect AUC (right panel)

3.2 Peak Filtering

The strategy here developed allowed flexible application of the pipeline to variable experimental conditions, such as the addition of multiple stimuli and the time of addition of the stimulus itself.

Through simplified equations designed on Microsoft Excel 2019 MSO, we could filter out residual noise and nonspecific signals thus performing a second step cleaning

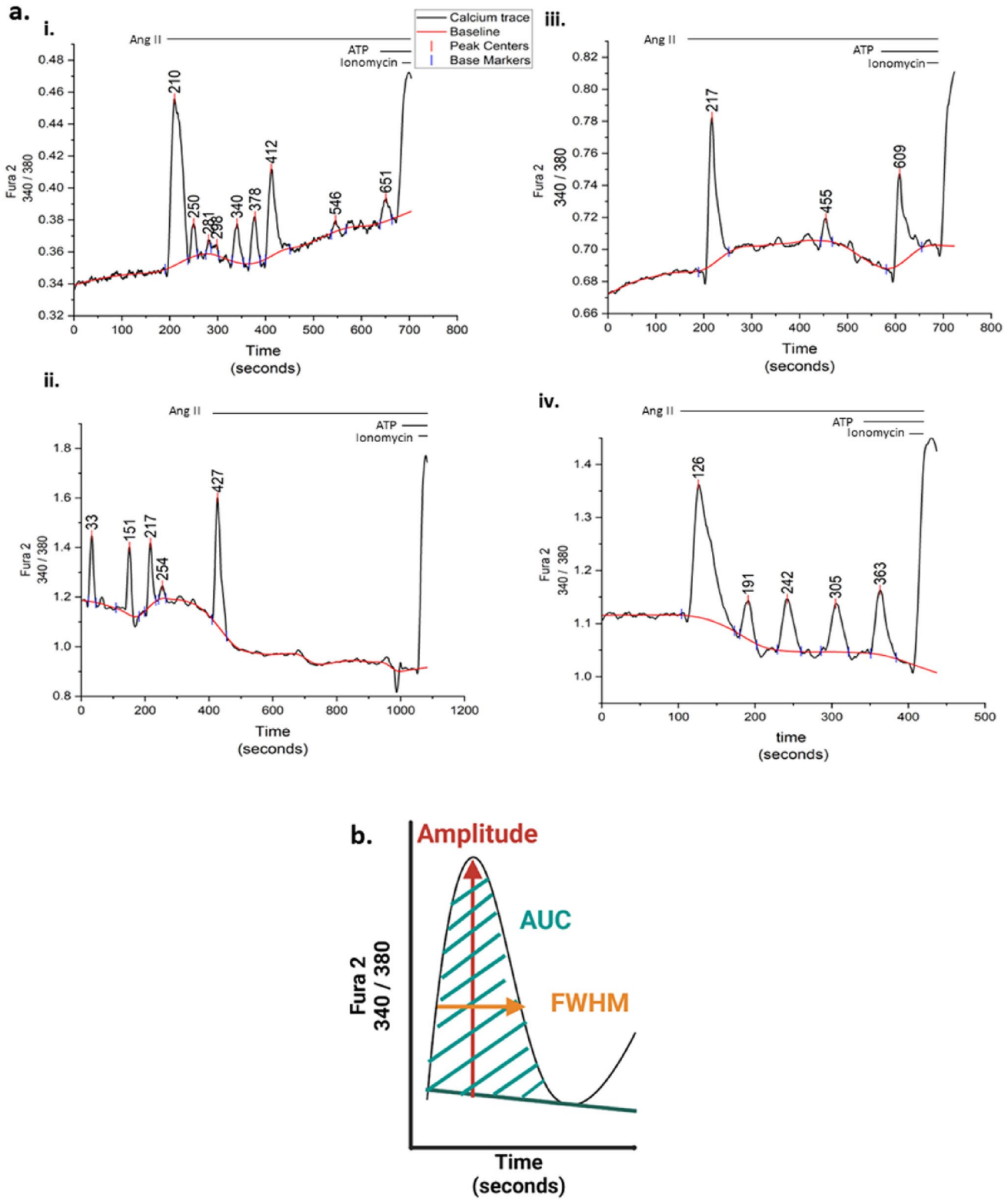

Fig. 4 Modeling human CD56+ AAC and APA cells intracellular Ca^{2+} dynamics by standardized peak detection and characterization. **a**. Baseline setting (red line) was adapted to the dynamic nature of the Ca^{2+} signals using the OriginPro 2023 OriginLab Corporation lab software as described in the peak detection algorithm settings. Ang II was used of [10 nM] to induce the Ca^{2+} peaks. ATP was used to induce non receptor mediated increase of $[Ca^{2+}]_i$. To confirm the cell responsiveness, ionomycin was used of [1μM]. Numbers on peaks represent the time in seconds at which each event has occurred. i + ii: AAC, iii + iv: APA. **b** Peak characterization was performed by calculating different features of each individual Ca^{2+} peak: amplitude (red line); full width at half maximum (FWHM, orange line); area under the curve (AUC, green area)

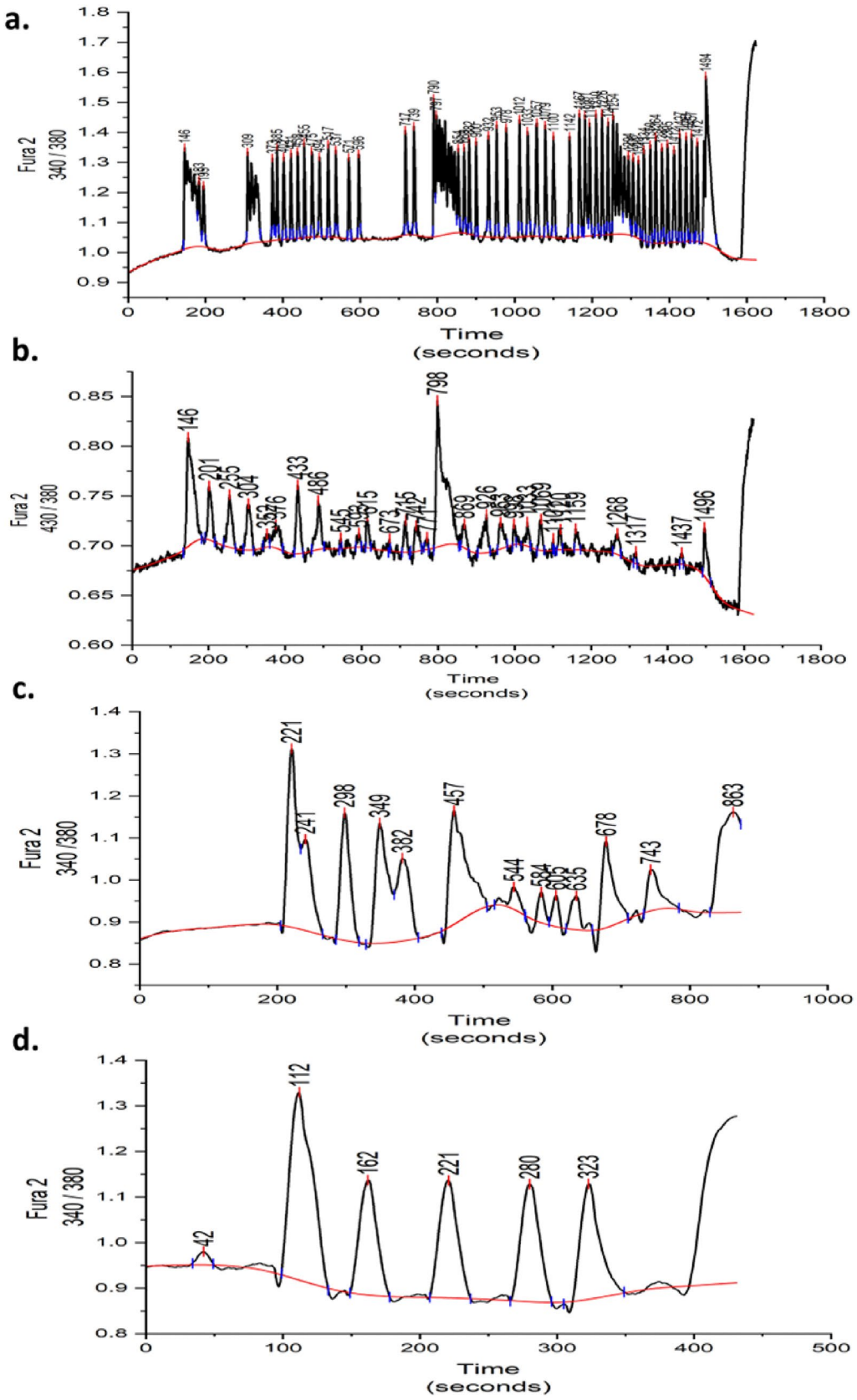
a.
Fura 2
340 / 380
Time
(seconds)
b.
Fura 2
430 / 380
Time
(seconds)
c.
Fura 2
340 /380
Time
(seconds)
d.
Fura 2
340 / 380
Time
(seconds)

◂**Fig. 5** Representative Ca^{2+} traces of AAC (**a**, **b**) and APA (**c**, **d**) cells with detection of Ca^{2+} peaks according to our pipeline. Algorithm developed shows flexibility and adjustability to different types of behaviors. Numbers on peaks represent the time in seconds at which each event has occurred

of the data, where peaks posing an area less than 0.5 combined with a height less than 0.016 were removed, using the following the equation:

$$= If((Area\ column < 0.5) * (height\ column < 0.016, \ ''Delete'')$$

The Ca^{2+} traces could be subdivided in various regions for subsequent detailed analysis according to the experimental procedure applied. Here, we defined a region where spontaneous intracellular Ca^{2+} activity occurs (i.e. before the addition of the stimulus) and a region where Ca^{2+} fluctuation occurs in response to the stimulus (Ang II-evoked peaks). The time of Ang II addition discriminates the two regions in the Ca^{2+} trace plot.

In case the addition of Ang II was provided at sec 130, the equation used is:

$$= If(timecell < 130, \ \ ''spon'', If(AND(timecell \geq 130, timecell < 260), \ \ ''10nMdose'', \ \ ''none''))$$

However, Ca^{2+} traces could adopt either a unique single Ca^{2+} transient behavior upon stimulus addition or an oscillatory behavior as depicted before in Figs. 3 And 4 [29]. In case of a multi peak behavior, it is applicable to segregate detected individual Ca^{2+} peaks in a time dependent manner to allow the differentiation between the first response transient and the subsequent peaks following this equation (with A3 and A2 demonstrating the number code of the cell);

$$= If\left(A3 = A2, OS(oscillating), \ ''First\ Peak''\right)$$

To be able to quantify the number of cells showing unique or a multi peak Ca^{2+} behavior, we employed the subtotal count function on Excel. As individual ROIs are indicated by different ROI-ID number, we sum all the detected peaks originating from 1 ROI using the distinct ID numbers and then we apply the following equation on the subtotal function results which resembles the number of ROIs showing oscillation activity with column I representing the subtotal count function results Supplementary file1.

$$= COUNTIF(I4 : I172, \ '' >= 2'')$$

Frequency of oscillations was also characterized when 2 or more peaks were detected (F= 1/T) (period=T represents time for one oscillation) (Fig. 6). To calculate the period (T), copy the Id index (ROI name) and index (Time) with the subtotal to a new sheet, then subtract each 2 consecutive row indexes ($= B4 - B3$). Remove nonspecific values resulting from data ID count by conditional formatting, highlighting cells, then pick the Text that contain (count). Filter out Column A (data Id ROIs) by color then Column C (T): by number, greater than 0. Continue to calculate the frequency in Hz(= 1/T).

Ca^{2+} signals plots were divided into resting conditions, in which spontaneous activity could be detected (light blue), and Ang II-stimulated conditions (light pink).

In our experiment, we used ATP (yellow) and ionomycin (light gray) as controls to determine the responsiveness and viability of the cells, thus the corresponding peaks were eliminated from detection by the algorithm (Fig. 6).

4 Discussion

We herein describe a novel pipeline methodology to analyze ex vivo Ca^{2+} imaging data of individual adrenocortical cells in a simple and reliable way. Thus far, many computational tools for analyzing intracellular Ca^{2+} changes that have been used require programming skills and knowledge of software languages and scripts [19–22] that are not familiar to a significant part of the biologists conducting experimental work [30, 31]. Therefore, the designed workflow described here represents a convenient approach to produce reproducible data and encourages autonomy of researcher with low or even zero prior bioinformatic skills.

The workflow of the pipeline provides an optimized protocol to use the algorithm embedded in the OriginPro 2023 software to promote the best peak detection approach. Processing data using Savitzky-Golay method (Windows 20) promotes a clear peak display of different Ca^{2+} behavior while it preserves small scaled peaks. The pipeline provides the optimum settings for baseline adjustment and peak identification algorithm to allow the analysis of irregular and complex patterns of Ca^{2+} kinetics associated with highly dynamic baseline drifts. The user is only left with the task of modifying the softwares settings without need of any code scripting, as herein described.

To allow detected peaks segmentation based on the time of stimuli addition, Microsoft Excel-based equations are designed. They require careful manual handling to ensure accurate peaks characteristics segregation.

It is worth noting that the OriginPro 2023 software already provides an App to analyze Ca^{2+} signals of patient-derived induced pluripotent stem cell cardiomyocytes (iPSC-CMs). However, as it requires an embedded Python and NumPy, SciPy libraries, and furnishes only an average information of all peaks per each assigned cell and not an assessment of individual peaks. Therefore, this approach isinadequate to provide a detailed detected-peaks analysis.

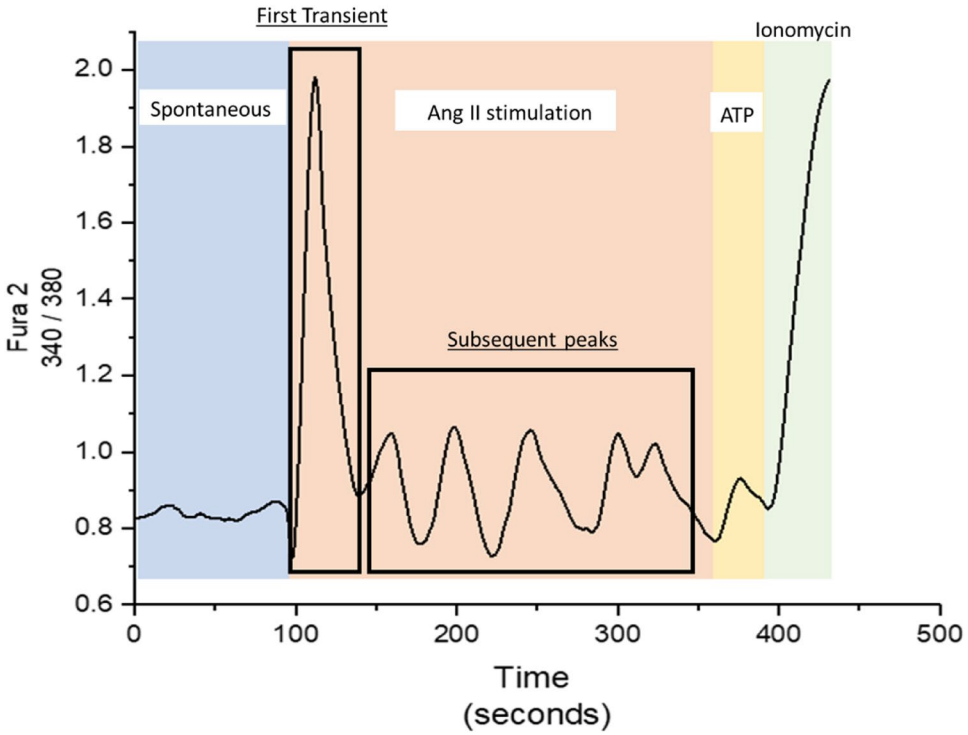

Fig. 6 Time defined segments of a single Ca^{2+} trace in CD56+ aldosterone-producing cell. All Ca^{2+} recordings followed the sequence shown: spontaneous phase (unstimulated conditions), Ang II-stimulated phase divided into first transient and subsequent peaks, ATP and ionomycin stimulated phases. Different segments are marked with different colors. Period of each phase differs for each slide of cells

The discussed analysis of intracellular Ca^{2+} fluctuations proved to be useful for investigating altered Ca^{2+} dynamics when applied to assess outputs of Ca^{2+} events in primary human cells isolated from aldosterone-producing adenoma (APA) and APA-adjacent (AAC) tissues of patients with PA, i.e. the most common curable form of arterial hypertension. It allowed to quantitatively monitor intracellular $[Ca^{2+}]_i$ fluctuations of isolated human CD56+ adrenocortical cells using the Ca^{2+}-sensitive indicator Fura-2 after Angiotensin II stimulation by a dynamic baseline drifting in order to process a large scale of heterogeneous data [4, 16, 32].

Thus, the methodology developed in this study uses reliable and easy to handle algorithms to track intracellular Ca^{2+}, with no requirement of scripts designing, thus abolishing the possibility of code scripting. This provides users with the ability to process datasets autonomously without prior programming knowledge. The simple approach offers the analysis of periodic and fading peaks. The settings of the peak detection algorithm are designed and tested to be highly efficient on various types of real time traces.

Importantly, the flexibility and robustness of the pipeline can be standardized across multiple studies as it yields non-subjective results and is applicable to large data sets and minimizes the possibility for human errors. The only con of our methodology is the inevitable need for manual handling, more specifically step 3, which includes the peak filtering Excel designed equations with careful operation, yet considered to be time efficient. Thus careful performance is required.

Of note, when we applied this methodology on our data set, we observed calcium behaviors upon Ang II stimulation that are reproducible in cells in close proximity. Our primary cells in culture show a very low proliferation rate and thus what we see in our experimental set up likely reflect the in vivo behavior. From dispersed $CD56^+$ adrenocortical cells, after 24 hours in culture, we did observe the formation of multicellular structures resembling the cyto-architecture of intact human adrenocortical glomeruli structures, the so called 'rosette". The functional behavior of cell assemblies, which were extensively studied and proven to coordinate Ang II-elicited calcium spikes in murine models [21, 33, 34], was not investigated in human CD56+ dispersed cells before and we are pleased to provide the scientific community with the method to analyse the crucial feature of acrenocortical cell biology.

Supplementary Information The online version contains supplementary material available at https://doi.org/10.1007/s40292-024-00641-5.

Acknowledgments Address all correspondence and requests for reprints to: Professor Gian Paolo Rossi, MD, FACC, FAHA, DIMED, Internal Medicine 4, University Hospital, via Giustiniani, 2, 35126 Padova, Italy. E-mail: gianpaolo.rossi@unipd.it.

Data availability The data that support the findings of this study are available on request from the corresponding author.

Declarations

Conflict of Interest The authors have nothing to declare.

Ethical Approval Research involved Human Participants who provided signed consents. The collection of samples was approved by the local ethics committee.

Funding Open access funding provided by Universit… degli Studi di Padova within the CRUI-CARE Agreement. This work was supported by research grants from the European Commission Marie Skłodowska-Curie Actions PhD program: MINDSHIFT (grant number 954798, website: http://www.eumindshift.eu).

References

1. Berridge MJ, Lipp P, Bootman MD. 2000-review-calcium signalling. Nat Rev. 2000;1:11–21.
2. Rizzuto R, De Stefani D, Raffaello A, Mammucari C. Mitochondria as sensors and regulators of calcium signalling. Nat Rev Mol Cell Biol. 2012;13:566–78.
3. Sneyd J, Han JM, Wang L, Chen J, Yang X, Tanimura A, et al. On the dynamical structure of calcium oscillations. Proc Natl Acad Sci U S A. 2017;114:1456–61.
4. Dupont G, Combettes L, Bird GS, Putney JW. Calcium oscillations. Cold Spring Harb Perspect Biol. 2011;3:1–18.
5. Sneyd J, Tsaneva-Atanasova K, Yule DI, Thompson JL, Shuttleworth TJ. Control of calcium oscillations by membrane fluxes. Proc Natl Acad Sci U S A. 2004;101:1392–6.
6. Bootman MD, Bultynck G. Fundamentals of cellular calcium signaling: a primer. Cold Spring Harb Perspect Biol. 2020;12:1–16.
7. Quinn SJ, Enyedi P, Tillotson DL, Williams GH. Cytosolic calcium and aldosterone response patterns of rat adrenal glomerulosa cells stimulated by vasopressin: comparison with angiotensin II. Endocrinology. 1990;127:541–8.
8. Qi H, Li X, Jin Z, Simmen T, Shuai J. The oscillation amplitude, not the frequency of cytosolic calcium, regulates apoptosis induction. iScience [Internet]. 2020;23:101671. https://doi.org/10.1016/j.isci.2020.101671.
9. Rossi GP. Primary aldosteronism: JACC state-of-the-art review. J Am Coll Cardiol [Internet]. 2019;74:2799–811. https://doi.org/10.1016/j.jacc.2019.09.057.
10. Scholl UI. Genetics of primary aldosteronism. Hypertension. 2022;79:887–97.
11. Iacobone M, Citton M, Viel G, Boetto R, Bonadio I, Tropea S, et al. Unilateral adrenal hyperplasia: a novel cause of surgically correctable primary hyperaldosteronism. Surg (United States) [Internet]. 2012;152:1248–55. https://doi.org/10.1016/j.surg.2012.08.042.
12. Williams GH. Aldosterone biosynthesis, regulation, and classical mechanism of action. Heart Fail Rev. 2005;10:7–13.
13. Yang T, He M, Zhang H, Barrett PQ, Hu C. L- And T-type calcium channels control aldosterone production from human adrenals. J Endocrinol. 2020;244:237–47.
14. Fernandes-Rosa FL, Boulkroun S, Zennaro MC. Genetic and genomic mechanisms of primary aldosteronism. Trends Mol Med [Internet]. 2020;26:819–32. https://doi.org/10.1016/j.molmed.2020.05.005.
15. Capponi AM, Lew PD, Jornot L, Vallotton MB. Correlation between cytosolic free Ca2+ and aldosterone production in bovine adrenal glomerulosa cells. Evidence for a difference in the mode of action of angiotensin II and potassium. J Biol Chem. 1984;259:8863–9.
16. Connor JA, Carter Cornwall M, Williams GH. Spatially resolved cytosolic calcium response to angiotensin II and potassium in rat glomerulosa cells measured by digital imaging techniques. J Biol Chem. 1987;262:2919–27.
17. Quinn SJ, Williams GH, Tillotson DL. Calcium oscillations in single adrenal glomerulosa cells stimulated by angiotensin II. Proc Natl Acad Sci U S A. 1988;85:5754–8.
18. Johnson EIM, Capponi AM, Vallotton MB. Cytosolic free calcium oscillates in single bovine adrenal glomerulosa cells in response to angiotensin II stimulation. J Endocrinol. 1989;122:391–402.
19. Gancayco CA, Gerding MR, Breault DT, Beenhakker MP, Barrett PQ, Guagliardo NA. Intrinsic adrenal TWIK-related acid-sensitive TASK Channel dysfunction produces spontaneous calcium oscillations sufficient to drive AngII (Angiotensin II)-unresponsive hyperaldosteronism. Hypertension. 2022;79:2552–64.
20. Seidel E, Schewe J, Zhang J, Dinh HA, Forslund SK, Markó L, et al. Enhanced Ca2+ signaling, mild primary aldosteronism, and hypertension in a familial hyperaldosteronism mouse model (Cacna1hM1560V/+). Proc Natl Acad Sci U S A. 2021;118 (17) e2014876118.
21. Guagliardo NA, Klein PM, Gancayco CA, Lu A, Leng S, Makarem RR, et al. Angiotensin II induces coordinated calcium bursts in aldosterone-producing adrenal rosettes. Nat Commun [Internet]. 2020;11:1–15. https://doi.org/10.1038/s41467-020-15408-4.
22. Wu X, Azizan EAB, Goodchild E, Garg S, Hagiyama M, Cabrera CP, et al. Somatic mutations of CADM1 in aldosterone-producing adenomas and gap junction-dependent regulation of aldosterone production. Nat Genet. 2023;55:1009–21.
23. Rossi GP, Lenzini L, Caroccia B, Rossitto G, Seccia TM. Angiotensin peptides in the regulation of adrenal cortical function. Explor Med. 2021;2:294–304.
24. Caroccia B, Fassina A, Seccia TM, Recarti C, Petrelli L, Belloni AS, et al. Isolation of human adrenocortical aldosterone-producing cells by a novel immunomagnetic beads method. Endocrinology. 2010;151:1375–80.
25. Grynkiewicz G, Poenie M, Tsien RY. A new generation of Ca2+ indicators with greatly improved fluorescence properties. J Biol Chem. 1985;260:3440–50.
26. Raposo-Neto JJ, Kowalski-Neto E, Luiz WB, Fonseca EA, Cedro AKCL, Singh MN, et al. Near-infrared spectroscopy with supervised machine learning as a screening tool for neutropenia. J Pers Med. 2023;14:9.
27. Savitzky A, Golay MJE. Smoothing and differentiation of data. Anal Chem [Internet]. 1964;36:1627–39. https://doi.org/10.1021/ac60214a047.
28. Gao C, Zhao P, Fan Q, Jing H, Dang R, Sun W, et al. Deep neural network: As the novel pipelines in multiple preprocessing for Raman spectroscopy. Spectrochim Acta Part A Mol Biomol Spectrosc [Internet]. 2023;302:123086. https://doi.org/10.1016/j.saa.2023.123086.

29. Christo SN, Diener KR, Hayball JD. The functional contribution of calcium ion flux heterogeneity in T cells. Immunol Cell Biol [Internet]. 2015;93:694–704. https://doi.org/10.1038/icb.2015.34.
30. Mariano D, Martins P, Helene Santos L, de Melo- Minardi RC. Introducing Programming Skills for Life Science Students. Biochem Mol Biol Educ. 2019;47:288–95.
31. Jamali N, Dobson ETA, Eliceiri KW, Carpenter AE, Cimini BA. 2020 BioImage Analysis Survey: community experiences and needs for the future. Biol Imaging. 2022;1:1–13.
32. Mackay L, Mikolajewicz N, Komarova S V., Khadra A. Systematic characterization of dynamic parameters of intracellular calcium signals. Front Physiol. 2016;7:525.
33. Leng S, Carlone DL, Guagliardo NA, Barrett PQ, Breault DT. Rosette morphology in zona glomerulosa formation and function. Mol Cell Endocrinol Internet. 2021;530:111287. https://doi.org/10.1016/j.mce.2021.111287.
34. Leng S, Pignatti E, Khetani RS, Shah MS, Xu S, Miao J, et al. β-Catenin and FGFR2 regulate postnatal rosette-based adrenocortical morphogenesis. Nat Commun [Internet]. 2020;11:1–14. https://doi.org/10.1038/s41467-020-15332-7.